Memoirs of the Faculty of Engineering, Nagoya University
Vol. 36, No. 2 (1984) — Research Report —

FLUID FLOW AND HEAT TRANSFER IN CORRUGATED WALL CHANNELS

RYOTARO IZUMI, HIROSHI YAMASHITA
and SADAMU KAGA

Department of Mechanical Engineering

(Received October 29, 1984)

Abstract

We investigate corrugated wall channels as a means of augmenting forced-convection heat transfer with single phase flow in heat exchangers. As the corrugated wall channels have simple structure and have direct effects on heat transfer due to heat transfer surface itself being bent, they are expected to have wide applications. Besides, as they can disturb the main current, they have extreme effects for the heat transfer augmentations. In order to find out adequate configurations of them, considering the model of parallel channel bent two times and that bent many times, we examine analytically and experimentally the fluid flow states and heat transfer characteristics of laminar flow and turbulent flow for various values of pitch P and bending angle θ, and try to make clear the mechanism of heat transfer augmentation. Particularly, we show aspects of flow such as impingement, deflection, separation, reattachment etc., local Nusselt number distributions, pressure losses and mean Nusselt number, indicate the effects of pitch and bending angle on them, and estimate the performance of corrugated wall channel as heat exchanger by area or volume goodness factors.

1. Introduction

An application of corrugated wall channel is examined as a means of augmenting the forced-convection heat transfer with a single-phase flow in heat exchangers. It is one of the passive augmentation techniques, which have no need for supply of power and have the effect of disturbing the main current itself without inserting devices in channels. Bergles[1, 2] gave outlines of earlier augmentation methods of

heat transfer and made a detailed comparison. Recently, applications of plate[3], orifice[4], blade[5], cylinder[6], etc.[7] as heat transfer promoters have been invesigated, but they make the structure complicated because of inserting them in the channel. Applications of rough surfaces with sand grain, rib[8] etc. have also been investigated, but they cannot disturb the main current itself because the height of roughness is not more than the thickness of boundary layer. On the contary, as corrugated wall channels have simple structures and have direct effects on heat transfer due to the heat transfer surface itself being bent, they are expected to have wide applications. Besides, as they can disturb the main current, they have extreme effects for the augmentation heat transfer.

Corrugated wall channels applied to plate heat exchangers were experimentally examined by Okada et al.[6, 9] They indicate that high heat transfer coefficients of plate heat exchangers were caused by repeating effects of the flow in the entrance region such as the expansion and contraction of the channel and changing the flow direction, but they didn't examine in detail the fluid flow and the mechanism of heat transfer. Peters et al.[10] and Suu et al[11, 12] examined fluid flow states in the channel bent only one time which was a part of corrugated wall channel, but they didn't examine heat transfer characteristics. The former treated the case of one quarter circular arc bending corner, and the latter was limited to the analysis by the potential theory. Moreover, the effect of pitch which is one of important geometrical parameters cannot be examined with the channel bent only one time. Sparrow et al.[13] examined in detail the distribution of local mass transfer coefficients in the channel bent three times by the naphtalene sublimation technique. But they paid attention mainly to the spanwise secondary flow, treated only one kind of channel shape and didn't examine adequate configurations for the augmentation heat transfer.

According to the above consideration, in order to find out adequate configurations of corrugated wall channels considering the model of parallel channel bent two times and that bent many times, we examine analytically and experimentally the fluid flow states and heat transfer characteristics of laminar flow and turbulent flow for various values of pitch P and bending angle θ. and try to make clear the mechanism of heat transfer augmentation. Particularly, we show aspects of flow such as impingement, deflection, separation, reattachment etc., local Nusselt number distributions, pressure losses and mean Nusselt number, indicate the effects of pitch and bending angle on them and estimate the performance of corrugated wall channel as heat exchanger by area or volume goodness factors[19~22].

Nomenclature

a : thermal diffusivity
a_φ, b_φ, c_φ, d_φ : coefficients
f_t : Fanning friction factor
H : channel width
h : heat transfer coefficient
IA, IAD, IB, IBD : positions in channel
j_H : Colburn heat transfer modulus
k : kinetic energy of turbulence

L : distance between bending corners
L' : length of neighborhood of bending region
L_c, L_v : corners of wall on the left-hand side
l : length scale of turbulence
Nu : Nusselt number
P : pitch
p : pressure
Pr : Prandtl number
Q : heat transfer augmentation
q : heat flux
R_c, R_v : corners of wall on the right-hand side
Re : Reynolds number
t : temperature
u : velocity
x_1, x_2 : coordinates
①, ②, ③ : divided zones in channel
θ : bending angle
λ : thermal conductivity
ν : kinematic viscosity
ρ : density
τ : shear stress
φ : dependent variable
ϕ : stream function
ω : vorticity

Subscripts

1 : in x_1 direction
2 : in x_2 direction
b : bulk
c : concave
in : inlet
m : mean
max : maximum
min : minimum
n : number of iterations
P : point at wall
s : starting point or straight tube
std : standard set of fluid property conditions
v : convex
w, $wall$: wall
$'$: dimensionless

2. Analysis and Experiment in the Case Where Channels Are Bent Two Times

2. 1. Numerical analysis

The analytical model is shown in Fig. 1, where H is the channel width, L is the distance between bending corners, $P \equiv L/H$ is the pitch and θ is the bending

angle. We call the walls on the right-hand side and the left-hand side towards the downstream R-side wall and L-side wall, and call the four corners R_v, R_c, L_v and L_c, where the subscripts v and c indicate the convex and the concave corner, respectively. We call the zone from the distance H upstream of the corner R_v to the distance H downstream of the corner L_v the neighborhood of bending region, and represent its length by L'. The inlet and the outlet of the channel are set up at the distance 200 times H away from the neighborhood of bending region. The values of pitch P vary from $P=0$ corresponding to the straight tube to a fairly large value $P=8$ showing a similar trend to the case of bending one time because of disappearance of interference between two bending regions. The values of bending angle θ vary from $\theta=0°$ corresponding to the straight tube to $\theta=90°$.

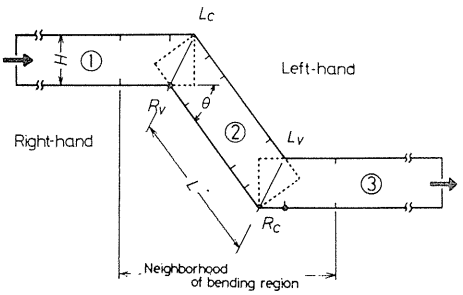

Fig. 1. Analytical model (1).

We divide the channel into three zones ①, ② and ③ with overlapping parts. We take Cartesian coordinates in each zone; x_1 is in the flow direction and x_2 is perpendicular to the wall.

Considering a steady incompressible laminar flow in the channel and constant physical properties of fluid, the basic equations for the stream function ψ (ψ is defined with $\rho u_1=\partial\psi/\partial x_2$ and $\rho u_2=-\partial\psi/\partial x_1$), the vorticity $\omega\equiv\partial u_2/\partial x_1-\partial u_1/\partial x_2$ and the temperature t are of the same type, and are written in the following dimensionless form[14];

$$a_\varphi\left\{\frac{\partial}{\partial x_1'}\left(\varphi\frac{\partial\psi'}{\partial x_2'}\right)-\frac{\partial}{\partial x_2'}\left(\varphi\frac{\partial\psi'}{\partial x_1'}\right)\right\}$$

$$-\frac{\partial}{\partial x_1'}\left\{b_\varphi\frac{\partial(c_\varphi\varphi)}{\partial x_1'}\right\}-\frac{\partial}{\partial x_2'}\left\{b_\varphi\frac{\partial(c_\varphi\varphi)}{\partial x_2'}\right\}+d_\varphi=0 \qquad (2.1)$$

where primes indicate dimensionless variables, φ is taken as dependent variables ψ' ω' and t'; and a_φ, b_φ, c_φ and d_φ are taken as standing for various functions. Dimensionless variables are as follows:

$$x_1'\equiv x_1/H,\quad x_2'\equiv x_2/H,$$

$$\psi'\equiv\psi/(\rho u_m H),\quad \omega'\equiv\omega/(u_m/H),$$

$$t'\equiv(t-t_{min})/(t_{max}-t_{min})\quad\text{or}\quad(t-t_{in})/(Hq_w/\lambda). \qquad (2.2)$$

and Reynolds number Re and Prandtl number Pr are as follows:

$$Re\equiv(u_m 2H)/\nu,\quad Pr\equiv\nu/a \qquad (2.3)$$

We calculate the case of $Re=0\sim2400$, $Pr=1$ or 0.71.

The boundary conditions are as following for ω', ψ' and t'. The flow is assumed to be hydrodynamically and thermally fully-developed at the inlet, except

the condition of t' under the constant heat flux condition, where the heat starting point is set up at the distance 5 times H upstream of the corner R_v and $t_{in}=0$. $\partial\varphi/\partial x_1$ is assumed to be zero at the outlet, except $\varphi=t'$ under the constant heat flux condition, where $\partial^2\varphi/\partial x_1^2=0$. At the walls, we impose the conditions for ω', ψ' and t' as follows:

$$\omega_P=-3(\psi_{NP}-\psi_P)/n_{NP}^2\rho-\omega_{NP}/2,\quad \psi_{min}=0 \text{ and } \psi_{max}=1,$$

$$t_{min}=0 \text{ and } t_{max}=1 \quad \text{and } q_w=\text{const.} \tag{2.4}$$

On the basis of these equations and boundary conditions, we calculate numerically by SOR iteration process, using the finite difference method by Gosman et al.[14] We almost take 1.0 for the values of the over-relaxation parameter, and set max $|\varphi_{ij}^n-\varphi_{ij}^{n-1}|<10^{-4}$ for the convergence criterion, where n is the number of iterations. The total numbers of x_1 and x_2 grid lines are 165 and 17 respectively. The grid distances are equal in the x_2 direction, but not equal in the x_1 direction except the neighborhood of bending region.

2. 2. Calculation results and discussions

(1) Streamlines The streamlines in the neighborhood of bending region for $P=3, \theta=90°$ and $Re=300$ are shown in Fig. 2. The values of stream function are indicated by the figures written alongside the streamlines, with 0 at R-side wall and 1 at L-side wall according to boundary conditions. The values less than 0 or more than 1 correspond to separation regions. The flow in the region away from the neighborhood of bending region is the plane Poiseuille flow in the same way as the straight tube, then u_1/u_m and ψ' are expressed as follows:

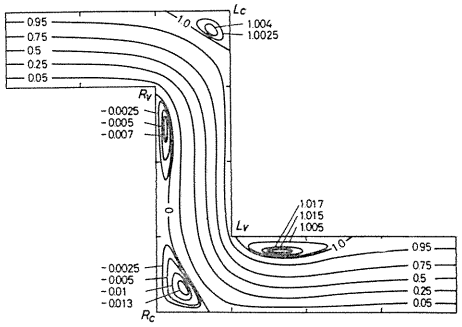

Fig. 2. Streamlines ($P=3$, $\theta=90°$, $Re=300$).

$$u_1/u_m=6x_2'(1-x_2'),\quad \psi'=\frac{\int_0^{x_2}\rho u_1 dx_2}{\rho u_m H}=6\left(\frac{x_2'^2}{2}-\frac{x_2'^3}{3}\right) \tag{2.5}$$

(2) Pressure contours and wall pressure distributions We show the aspects of pressure in Figs. 3(a) and (b). Figure 3(a) shows the pressure contours in the neighborhood of bending region in solid lines and dashed lines and with figures written alongside the curved lines indicate the pressure coefficients $(p-p_s)/\{(1/2)\rho u_m^2\}$, where p_s is the standard pressure at the position S which is the center of the cross section at the distance H upstream of the corner R_v. Figure 3(b) shows the distributions in the flow direction of the pressure at both walls; the solid line and the dashed line correspond to R-side wall and L-side wall, and the chain line indicates the pressure distribution in the straight tube, in which the pressure loss Δp_s in the distance $\Delta x_1=H$ is as follows[15]:

$$\frac{\Delta p_s}{(1/2)\rho u_m^2}=\frac{48}{Re}\frac{\Delta x_1}{H}=\frac{48}{Re} \tag{2.6}$$

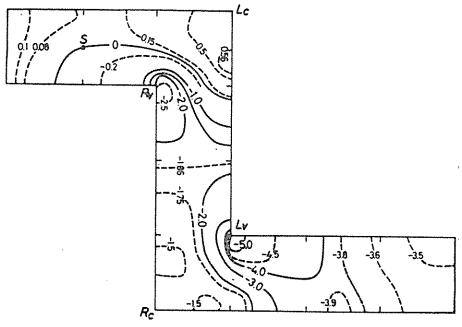

(a) Pressure contours ($P=3$, $\theta=90°$, $Re=300$).

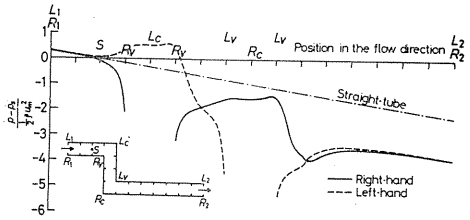

(b) Wall pressure distributions ($P=3$, $\theta=90°$, $Re=300$).

Fig. 3.

The pressure contours are complicated in the neighborhood of bending region. The pressure varies abruptly near the convex corners L_v and R_v, and it has uniform distributions with rather high values in the separation zones near the concave corners L_c and R_c and descends abruptly at immediate downstream there of. Besides, it change with the same falling gradient as straight tube at a long distance from the bending region.

(3) Local Nusselt number distributions in the case of constant wall temperature condition We give $t_{min}=0$ for R-side wall and $t_{max}=1$ for L-side wall as shown in Section 2. 1. In this case, for the straight tube, the temperature distribution is independent of Reynolds number and linear in the direction perpendicular to the wall, and does not change in the flow direction. Thus, the bulk temperature t_b does not change in the flow direction, and we obtain $t_b=(1/2)(t_{max}+t_{min})$ and $\partial t/\partial x_2=(t_{max}-t_{min})/H$. Moreover, we obtain the local Nusselt number Nu, which is independent of Reynolds number and constant in the whole channel, as follows[16]:

$$Nu\equiv\frac{h2H}{\lambda}=\frac{|\partial t/\partial x_2|_{wall}2H}{|t_w-t_b|} \tag{2.7}$$

This condition simplifies the results in the case of the straight tube, and is suitable for estimation of the heat transfer augmentations in the corrugated wall channels. Though the bulk temperature is undetermined in the neighborhood of the bending region where the flow is disturbed, it can be approximated by the equation $t_b=(1/2)(t_{max}+t_{min})$, so that the Nusselt number is defined by the same equation in the case of the straight tube.

We show the local Nusselt number distributions in Figs. 4(a) and (b) corresponding to R-side wall and L-side wall, respectively. We take the position in the flow direction as the abscissa, with the symbols R_v, R_c, L_v and L_c for the corners and the arrows for neighborhood of the bending region, and we take Reynolds numbers $Re=0$, 75, 300, 600 and 1200 as the parameter. For $Re=0$, where the heat convection is nonexistent, Nusselt number has the maxima at the convex corners

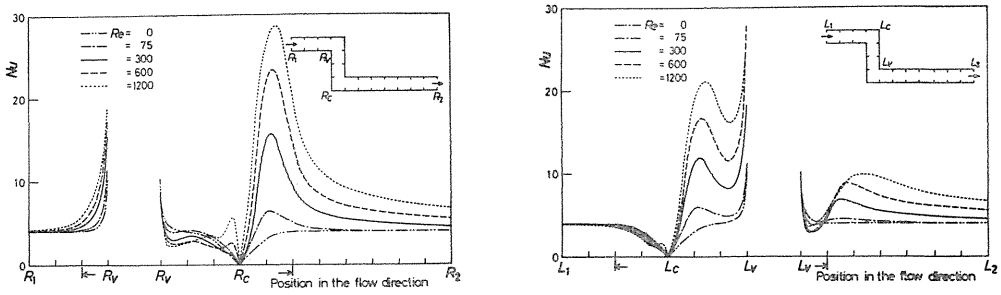

(a) R-side wall (b) L-side wall

Fig. 4. Local Nusselt number distributions.
(constant temperature condition, $P=3$, $\theta=90°$).

R_v and L_v, and the minima at the concave corners R_c and L_c, and its value approaches 4, which is the value in the case of the straight tube, at a long distance from the corners. Moreover, its distribution is independent of the flow direction and symmetric with respect to the center of bending region. For relatively small Reynolds number $Re=75$, Nusselt numbers at corresponding positions in two bending regions are almost equal to each other, in the same manner as the case of fluid flow states, due to the absence of the interference of two bending regions. For large Reynolds number, Nusselt numbers are very large at the positions where the flow impinges, and slightly large at the immediate upstream of the corners R_v and L_v where the flow deflects toward one side and at the immediate downstream of the corner L_v where the flow reattaches. The effect of bending remains to fairly far downstream, and Nusselt numbers are large over a wide region. Nusselt number distributions are almost the same as wall shear stress distributions. Nusselt number distributions vary fairly with the pitch. Particularly, for $P=2$, the value is large and the effect of bending remains to the farthest downstream.

(4) Local Nusselt number distributions in the case of constant heat flux condition In this case, the effects of the heat starting point and the bending overlap each other. The local Nusselt number is defined as follows:

$$Nu \equiv \frac{h2H}{\lambda} = \frac{(q_w/\lambda)2H}{|t_w - t_b|} \qquad (2.8)$$

where the bulk temperature t_b is calculated assuming that the fluid flows regularly without a separation, and holds all the heat quantity between the heat starting point and the considered point. Figure 5 shows the local Nusselt number distributions for $P=3$, $Re=300$ and 1000. It has the same trend as that described in the case of constant wall temperature condition.

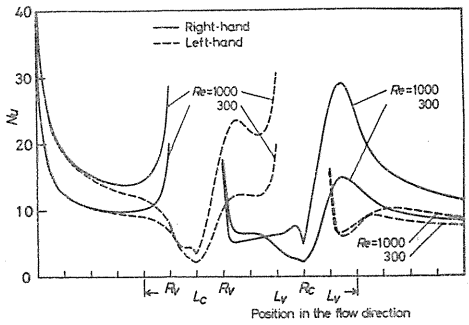

Fig. 5. Local Nusselt number distributions (constant heat flux condition, $P=3$, $\theta=90°$).

2. 3. *Experimental apparatus and procedure*

The outline of the apparatus used in this experiment is as follows. The rectangular channel of 150mm×30mm cross section was formed with a 20mm thick bakelite and set in a horizontal position. The heat transfer surface was made of a 30μm thick stainless steel foil attached on the bakelite, and it was heated electrically so that the heat flux q was constant. The surface temperatures were measured by a lot of copper constantan thermocouples of 100μm diameter put between the bakelite and stainless steel foil.

2. 4. *Experimental results and discussions*

(1) Local Nusselt number distributions We show the local Nusselt number distributions in Figs. 6 and 7. Figures 6(a) and (b) show the effects of Reynolds number Re for $P=3$ and $\tan(\theta/2)=3/4$, corresponding to R-side wall and L-side wall, respectively. Figures 7(a) and (b) show the effects of the bending angle θ

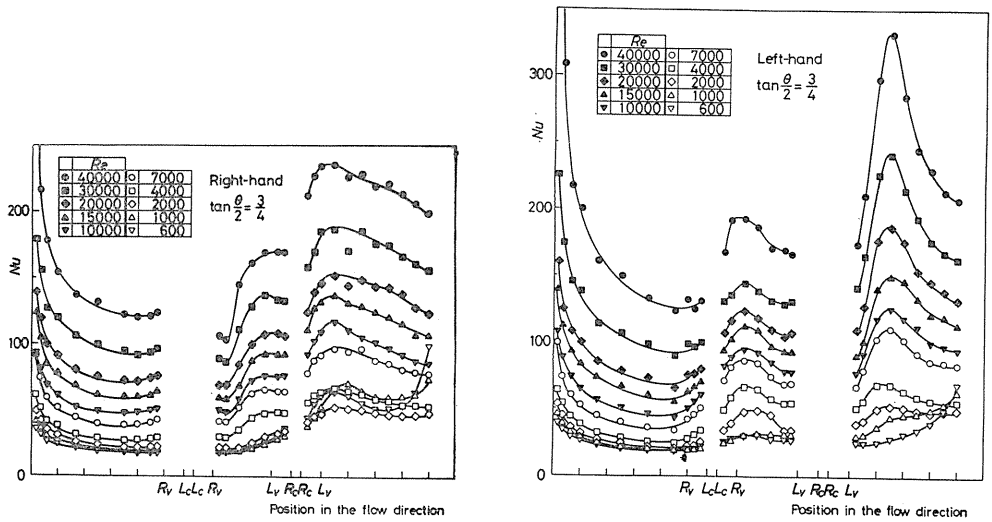

(a) R-side wall ($P=3$, $\tan(\theta/2)=3/4$) (b) L-side wall ($P=3$, $\tan(\theta/2)=3/4$)

Fig. 6. Local Nusselt number distributions (Effects of Reynolds number).

for $P=3$ and $Re=20000$, corresponding to R-side wall and L-side wall, respectively. Nusselt numbers have the maxima near the impinging points and the reattaching points in both sides of the channel walls. In contrast with the analytical results for laminar flow (see Figs. 4 and 5), it is clear that the maxima near the reattaching points are very large due to the effect of turbulence in the separating shear layer. The Nusselt numbers in the downstream of the second bending corners increase as the increase of bending angle.

(2) Mean Nusselt numbers We show the relations between mean Nusselt number over the neighborhood of bending region and Reynolds number in Figs. 8(a) and (b) for $P=3$ and $\theta=0°\sim90°$, corresponding to R-side wall and L-side wall, respectively.

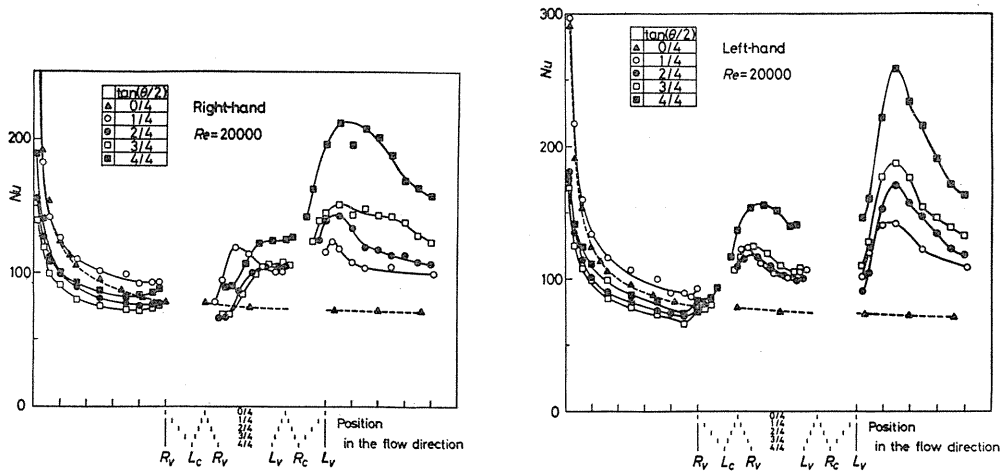

(a) R-side wall ($P=3$, $Re=20000$) (b) L-side wall ($P=3$, $Re=20000$)

Fig. 7. Local Nusselt number distributions (Effects of bending angle).

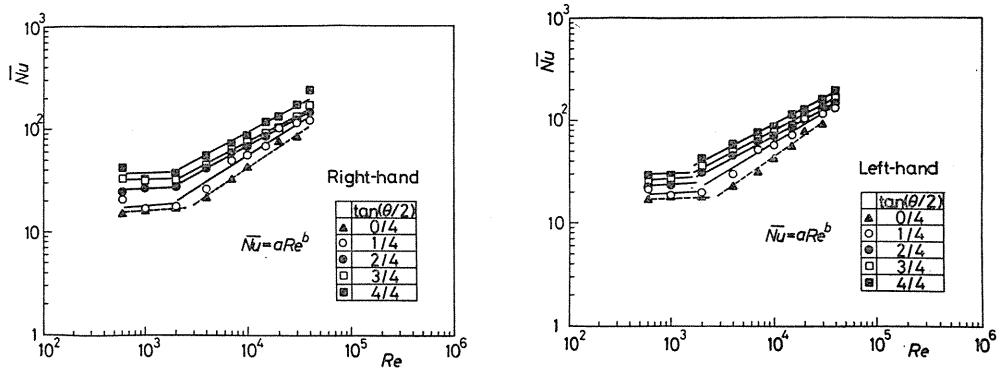

(a) R-side wall ($P=3$) (b) L-side wall ($P=3$)

Fig. 8. Mean Nusselt numbers.

3. Analysis in the Case Where Channels Are Bent Many Times

3. 1. Numerical analysis

The analytical model is shown in Fig. 9. The calculation is performed in the range between the positions IA and IBD, and "repeating conditions" are applied to the boundaries IA and IBD. The calculation methods are almost similar to the case of bending two times, but as two-equatinn model is applied for turbulent flow, two dependent variables are added to φ in the basic equation; the kinetic energy of turbulence $k \equiv (1/2)\overline{u_i' u_i'}$ and the product k and the length scale of turbulence kl[14, 17].

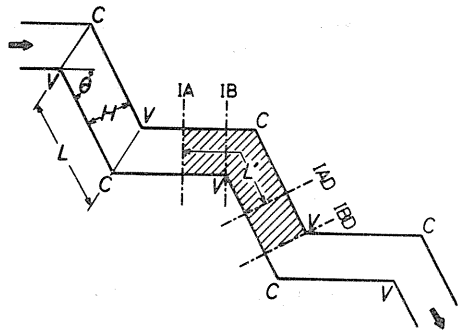

Fig. 9. Analytical model (2).

3. 2. Calculation results and discussions

(1) Case of the laminar flows The examples of streamlines for $Re=300$ are shown in Figs. 10(a), (b), (c) and (d). The effects of the pitch P and the bending angle θ on the pressure losses, the heat transfer quantities and the goodness factors are shown in Figs. 11 and 12. Figure 11(a) shows the total pressure losses

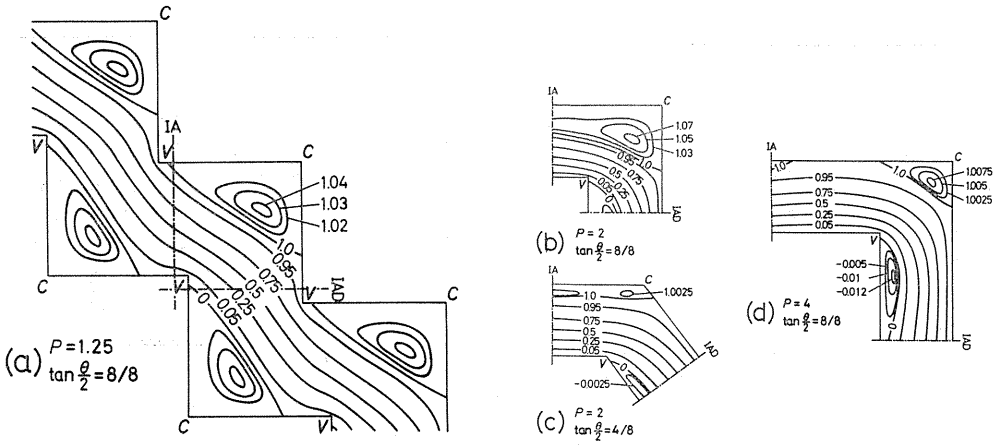

Fig. 10. Streamlines ($Re=300$, bending many times).

and the pressure losses due to bending in terms of the Fanning coefficients f_t and f. Figure 11(b) shows mean Nusselt number $\overline{Nu}$ and Colburn's j factor j_H. In those figures, the curved lines pass through a maximum at the position $P\fallingdotseq 2$, and they are asymptotic for $P>4$. For a small value of θ, f_t and $\overline{Nu}$ have very small values, especially for $\theta=0°$, $f_t=0.08$ and $\overline{Nu}=8.235$, but the curves of f_t and $\overline{Nu}$ increase abruptly at the positions of $\tan(\theta/2)\fallingdotseq 2/8$ and $\tan(\theta/2)\fallingdotseq 5/8$, respectively. Figure 11(c) shows the area goodness factor j_H/f_t. The values are mostly small compared with the values for straight tube. Figure 12 shows the volume goodness factor, that is, the plot of heat transfer coefficient h_{std} and fluid pumping power per unit of surface area E_{std}[18]. Solid lines indicate the case of $P=2$, $\tan(\theta/2)=2/8$ or $8/8$ and various values of Reynolds number written alongside the curves. Broken lines indicate the case of $Re=300$, $\tan(\theta/2)=8/8$ and various values of

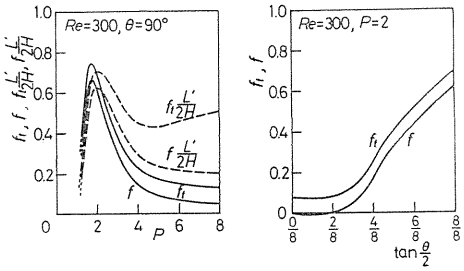

(a) Pressure losses

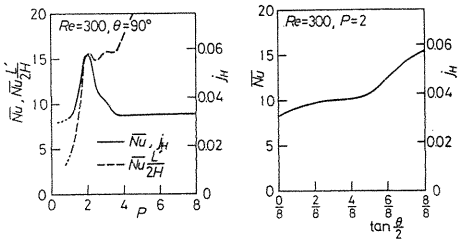

(b) Heat transfer quantities

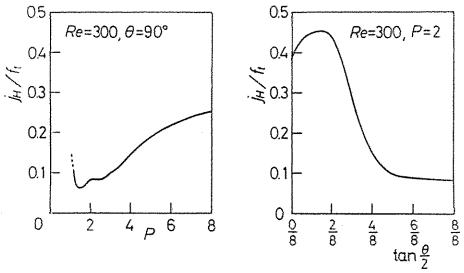

(c) Area goodness factor

Fig. 11. Effects of pitch and bending angle (Re=300, bending many times).

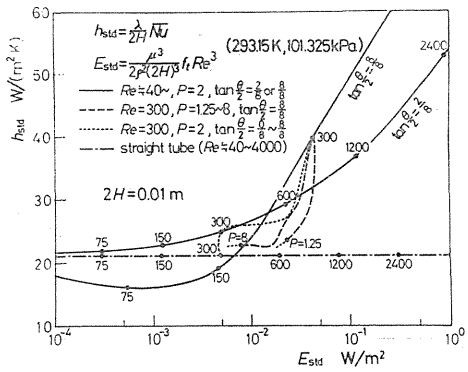

Fig. 12. Volume goodness factor (laminar flow, bending many times).

pitch. Dotted lines indicate the case of Re=300, P=2 and various values of bending angle. A dot-dash-line indicates the case of the straight tube. It is obvious that the performance of corrugated wall channels is more excellent in the case of tan ($\theta/2$)=2/8 for $E_{std}<1.5\times10^{-2}$W/m^2 and tan ($\theta/2$)=8/8 for $E_{std}>1.5\times10^{-2}$W/m^2.

(2) Case of the turbulent flows The distributions of the turbulent kinetic energy $k/(1/2)u_m^2$ and the length scale of turbulence l/H are shown with solid lines in Figs. 13 and 14, where (a) and (b) are the cases of bending many times and (c) are the case of bending one time. The dotted lines and the dot-dash-lines

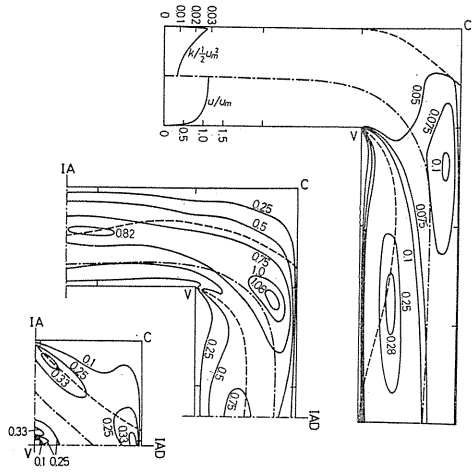

(a) Bending many times (P=1.109)
(b) Bending many times (P=3.625)
(c) Bending one time

Fig. 13. Distributions of the turbulent kinetic energy $k/(1/2)u_m^2$ (Re=40000).

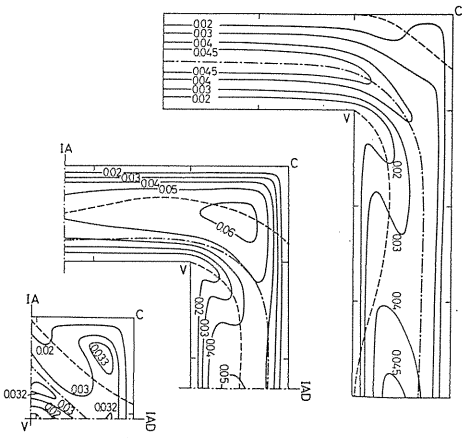

(a) Bending many times (P=1.109)
(b) Bending many times (P=3.625)
(c) Bending one time

Fig. 14. Distributions of the length scale of turbulence l/H (Re=40000).

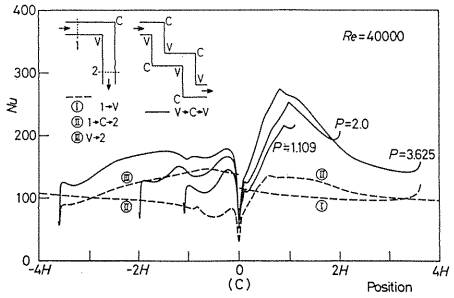

Fig. 15. Local Nusselt number distributions (Re=40000).

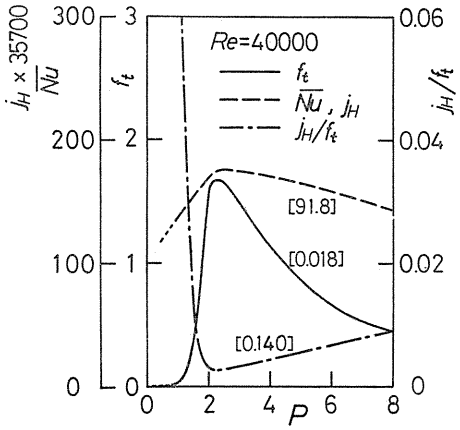

Fig. 16. Effects of pitch on f_t, $\overline{Nu}$ and j_H/f_t (Re=40000).

indicate the separation regions and the center streamlines, respectively. The cross distributions of $k/(1/2)u_m^2$ and u/u_m, which are used as inlet boundary condition in the case of bending one time, are illustrated at the extreme upperstream side of channel in Fig. 13(c). The kinetic energy k is large in the neighborhood of flow impinging point and separating shear layer at the immediate downstream of the corner V, but small near the corner C. The length scale l increases approximately proportionally to the distance from the wall except near the corner V where the

area in which l value is small extends along the separating shear layer, and it is large in the middle of the channel, especially in the center of the bending region. We show the local Nusselt number distributions in Fig. 15, where the solid lines and the dashed lines correspond to the case of bending many times ($P=1.109$, 2.0 and 3.625) and bending one time, respectively. We illustrate the curves in the latter case fitting in with those for $P=3.625$, and number them in terms of Ⅰ, Ⅱ, Ⅲ from the upper stream. It is clear that Nusselt numbers are very large near the reattaching points in agreement with the measurement for turbulence (See Figs. 6 and 7). We show the effects of pitch on the Fanning coefficient f_t, the mean Nusselt number $\overline{Nu}$ (j_H) and the area goodness factor j_H/f_t in Fig. 16 where the figures in the brackets indicate the corresponding values for the straight tube. f_t and $\overline{Nu}$ have the maximum at $P\fallingdotseq 2.3$, and j_H/f_t has the minimum at the same value of P.

4. Conclusions

We consider the model of parallel wall channel bent two times and that bent many times in order to find out adequate configurations of corrugated wall channels, and examine analytically and experimentally the fluid flow states and heat transfer characteristics of laminar flow and turbulent flow for various values of pitch P and bending angle θ. The results are summarized as follows:

(1) In the case of bending two times;

We divided the channel into three zones with overlapping parts, and calculated numerically by applying the finite difference method to each zone and combining the values in the overlapping parts. We showed streamlines, pressure contours, local Nusselt numbers and mean Nusselt numbers for $P=0\sim8$, $\theta=0°\sim90°$ and $Re=0\sim40000$. The fluid flow states and the heat transfer characteristics vary fairly with Reynolds number, the pitch and the bending angle. For large Reynolds number, the effect of bending is large and the interference of two bending regions is intense. The effect of bending has maximum at a specified value of pitch dependent on Reynolds number, such as $P\fallingdotseq 2$ for $Re=300$. The Nusselt numbers in the downstream of the second bending corners increase as the increase of bending angle.

(2) In the case of bending many times;

We calculated by finite difference method similar to the case of bending two times with adequate repeating boundary conditions, and applied two-equation model (k-kl) for a turbulent flow. We showed streamlines, pressure losses, heat transfer quantity and distributions of the turbulent kinetic energy and length scale of turbulence, for $P=1\sim8$, $\theta=0°\sim90°$ and $Re=0\sim2400$ or for $P=1\sim8$, $\theta=90°$ and $Re=40000$. Moreover, we estimate the performance of corrugated wall channel as heat exchanger by area or volume goodness factors.

Acknowledgement

This work was supported by the Grant-in-Aid for Fundamental Scientific Research from the Ministry of Education of the Japanese government. We are

grateful to Dr. Kenyu Oyakawa, Associate Professor of Ryukyu University for his cooperations. We are also grateful to Mr. Akio Fujishiro for his help in the experiments. The numerical calculations in this report were carried out with FACOM 230-75 and M-200 Computer at Nagoya University Computer Center.

References

1) Bergles, A. E., Progress in Heat and Mass Transfer I, (1969), 331, Pergamon Press.
2) Bergles, A. E., Applied Mechanics Reviews, 26-6 (1973-6), 675.
3) Cur, N. and Sparrow, E. M., Int. J. Heat Mass Transfer, 21-8 (1978-8), 1069.
4) Koram, K. K. and Sparrow, E. M., Trans. ASME, Ser. C, 100-4 (1978-11), 588.
5) Ishiki, N. and Takenouchi, Y., 11th National Heat Transfer Symposium of Japan (in Japanese), (1974-5), 457.
6) Konno, H. et al., Kagaku Kogaku (in Japanese), 31-9 (1967-9), 872.
7) Maesawa, S., et al., 13th National Heat Transfer Symposium of Japan (in Japanese), (1976-5), 103.
8) Han, J. C., et al., Int. J. Heat Mass Transfer, 21-8 (1978-8), 1143.
9) Okada, K., et al., Kagaku Kogaku (in Japanese), 32-11 (1968-11), 1127.
10) Hurd, A. C. and Peters, A. R., Trans. ASME, Ser. D, 92-4 (1970-12), 908.
11) Suu, T. and Fujii, K., Trans. Society of Heating, Air-Conditioning and Sanitary Engineers of Japan (in Japanese), 5 (1977-10), 11.
12) Suu, T. and Fujii, K., page 21 of Reference (11).
13) Goldstein, L. Jr and Sparrow, E. M., Trans. ASME, Ser. C, 99-2 (1977-5), 187.
14) Gosman, A. D., et al., Heat and Mass Transfer in Recirculating Flow, (1969), Academic Press.
15) Tomita, Y., Introduction to Fluid Dynamics (in Japanese), (1971), 166, Yokendo.
16) Shah, R. K. and London, A. L., Advances in Heat Transfer, Supplement 1, Laminar Flow Forced Convection in Ducts, (1978), 153, Academic Press.
17) Launder, B. E. and Spalding, D. B., Mathematical Models of Turbulence, (1972), 100, Academic Press.
18) page 393 of Reference (16).
19) Izumi, R., et al., Bulletin of the JSME, 24-194 (1981-8), 1425.
20) Izumi, R., et al., Bulletin of the JSME, 24-198 (1981-12), 2098.
21) Izumi, R., et al., Bulletin of the JSME, 26-216 (1983-6), 1027.
22) Izumi, R., et al., Bulletin of the JSME, 26-217 (1983-7), 1146.